Near-Infrared Fluorescent Proteins : Multiplexing and Optogenetics across Scales

Shcherbakova, Daria M.

2018-12

Shcherbakova , D M , Stepanenko , O V , Turoverov , K K & Verkhusha , V V 2018 , ' Near-Infrared Fluorescent Proteins : Multiplexing and Optogenetics across Scales ' , Trends in Biotechnology , vol. 36 , no. 12 , pp. 1230-1243 . https://doi.org/10.1016/j.tibtech.2018.06.011

http://hdl.handle.net/10138/308989
https://doi.org/10.1016/j.tibtech.2018.06.011

publishedVersion

Trends in Biotechnology

CellPress
REVIEWS

Review

Near-Infrared Fluorescent Proteins: Multiplexing and Optogenetics across Scales

Daria M. Shcherbakova,[1] Olesya V. Stepanenko,[2] Konstantin K. Turoverov,[2,3] and Vladislav V. Verkhusha[1,4,*]

Since mammalian tissue is relatively transparent to near-infrared (NIR) light, NIR fluorescent proteins (FPs) engineered from bacterial phytochromes have become widely used probes for non-invasive *in vivo* imaging. Recently, these genetically encoded NIR probes have been substantially improved, enabling imaging experiments that were not possible previously. Here, we discuss the use of monomeric NIR FPs and NIR biosensors for multiplexed imaging with common visible GFP-based probes and blue light-activatable optogenetic tools. These NIR probes are suitable for visualization of functional activities from molecular to organismal levels. In combination with advanced imaging techniques, such as two-photon microscopy with adaptive optics, photoacoustic tomography and its recent modification reversibly switchable photoacoustic computed tomography, NIR probes allow subcellular resolution at millimeter depths.

Highlights

New monomeric NIR fluorescent proteins (FPs) complement GFP-like FPs for cross-talk-free imaging. Spectrally distinct versions of these FPs are available, ranging from 670 to 720 nm in emission maxima.

The first NIR FRET biosensor, which detects Rac1 GTPase, is compatible with simultaneous imaging with CFP-YFP-based biosensors.

Because they have excitation and fluorescence close to or within the NIR window of tissue transparency (650–900 nm), NIR probes can be imaged across scales from subcellular to whole animals. Functional imaging is possible using cell signaling, cell cycle, and protein–protein interaction reporters.

Spectral properties of NIR FPs combined with advanced imaging approaches, such as structured illumination, two-photon microscopy, and photoacoustic tomography, enable subcellular resolution at millimeter depths.

Monomeric NIR FPs and Biosensors Open New Possibilities for Imaging and Optogenetics

NIR FPs derived from **bacterial phytochrome photoreceptors(BphPs)** (see Glossary) are useful probes for imaging across spatial scales from subcellular to whole body. In microscopy, NIR FPs allow spectral multiplexing with FPs of the GFP family and **optogenetic** tools activated by blue light. In *in vivo* imaging, deep penetration of NIR light in tissue, low autofluorescence, and reduced scattering in NIR make NIR FPs superior to GFP-like FPs (reviewed in [1]). NIR FPs have been widely used in various fields of biology and biomedicine, including cancer research [2–7], neuroscience [8–10], stem cell studies [11–13], parasitology [14], and virology [15], wherein the probes' NIR spectra allow their non-invasive visualization *in vivo* or labeling of organelles and cells for multicolor imaging.

Most NIR FPs are engineered that bind the PAS and GAF domains of BphPs. As chromophores, bacterial phytochromes use biliverdin (BV), which is available in mammalian cells as a product of heme breakdown. Currently, there are about 20 different NIR FPs developed from bacterial phytochromes that can be grouped in series named by their developers: iRFPs [16,17] and miRFPs [18,19], IFPs [20,21] and mIFP [22], and Wi-Phy [23]. The m/iRFP and m/IFP series, which were tested for their performance in mammalian cells, differ in their molecular brightness, effective brightness when expressed in mammalian cells (**cellular brightness**), spectral properties, and oligomeric state (Table 1, Key Table). A recent NIR FP developed from cyanobacterial phycobiliprotein photoreceptor smURFP [24] is considerably dimmer than iRFPs [25], although it is an interesting engineering result showing that a photoreceptor may be evolved to bind BV autocatalytically.

[1]Department of Anatomy and Structural Biology and Gruss-Lipper Biophotonics Center, Albert Einstein College of Medicine, Bronx, NY 10461, USA
[2]Laboratory of Structural Dynamics, Stability and Folding of Proteins, Institute of Cytology, Russian Academy of Sciences, St. Petersburg 194064, Russian Federation
[3]Department of Biophysics, Peter the Great St. Petersburg Polytechnic University, St. Petersburg 195251, Russian Federation
[4]Department of Biochemistry and Developmental Biology, Faculty of Medicine, University of Helsinki, Helsinki 00290, Finland
*Correspondence: vladislav.verkhusha@einstein.yu.edu (V.V. Verkhusha).

 https://doi.org/10.1016/j.tibtech.2018.06.011

Key Table

Table 1. BphP-Derived NIR FPs with Demonstrated *In Vivo* and Live-Cell Applications and Far-Red GFP-like FPs

NIR FP	Excitation (nm)	Emission (nm)	Extinction coefficient ($M^{-1}cm^{-1}$)	Quantum yield (%)	Molecular brightness[a]	Molecular brightness versus iRFP713 (%)	Oligomeric state	Photostability in mammalian cells, $t_{1/2}$ (s)	pK_a	Brightness in HeLa cells versus iRFP713 (%)[b]	Refs
miRFP670	642	670	87 400	14.0	12.2	198	Monomer	490 (155)	4.5	72	[18]
miRFP703	674	703	90 900	8.6	7.8	127		650 (394)	4.5	37	
miRFP709	683	709	78 400	5.4	4.2	69		500 (192)	4.5	30	
mIFP[b,c]	683 (683)	705 (704)	65 900 (82 000)	6.9 (8.4)	4.6	74		90 (54)	4.5	15	[22]
IFP2.0[b,c]	688 (690)	709 (711)	72 900 (98 000)	6.8 (8.1)	5.0	80	Dimer[d]	150 (108)	4.5	8	[21,22]
iRFP670	643	670	114 000	12.2	13.9	225	Dimer	290	4.5	119	[17,21]
iRFP682	663	682	90 000	11.1	10.0	162		490	4.5	105	
iRFP702	673	702	93 000	8.2	7.6	124		630	4.5	61	
iRFP713 (aka iRFP)	690	713	98 000	6.3	6.2	100		960	4.5	100	[16]
iRFP720	702	720	96 000	6.0	5.8	93		490	4.5	112	[16,17]
miRFP670-2	643	670	103 000	13.6	14.0	227	Monomer	310	4.5	72	[29]
miRFP682	663	682	91 000	11.2	10.2	165		500	4.5	117	
miRFP702	673	702	88 000	8.1	7.1	115		640	4.5	37	
miRFP713	690	713	99 000	7.0	6.9	112		980	4.5	109	
miRFP720	702	720	98 000	6.1	6.0	97		510	4.5	116	[19]
mCherry[e]	587	610	72 000	22.0	15.8	255	Monomer	NA[f]	3.8	NA	[19,28]
FusionRed[e]	580	608	83 000	19.0	15.8	255		NA	4.6	NA	[28,37]
mNeptune[e]	600	650	57 500	20.0	11.5	185	Dimer[g]	NA	5.4	NA	[37,72,73]
mCardinal[e]	603	651	79 000	18.0	14.2	229		NA	5.3	NA	[72–74]

[a]Determined as a product of extinction coefficient at excitation maximum (in $mM^{-1}cm^{-1}$) and fluorescence quantum yield.
[b]Determined as an effective NIR fluorescence in transiently transfected live HeLa cells with no supply of exogenous BV and after normalization to fluorescence of co-transfected EGFP and overlap of FP spectra with excitation laser and emission filters.
[c]Characteristics of NIR FPs shown in original publications are in parentheses.
[d]Originally reported as a monomer, IFP2.0 was later found to be a dimer [22].
[e]Far-red GFP-like FP.
[f]NA, not available.
[g]Originally reported as monomers, mNeptune and mCardinal were later found to be dimers [73].

Relatively low quantum yield of NIR FPs is compensated by their high extinction coefficient. The resulting molecular brightness of NIR FPs is comparable to modern far-red FPs of the GFP family (Table 1). NIR FPs are used in microscopy in the same constructs and imaging conditions as GFP-like probes. However, it is important to use light sources that produce adequate light intensities in NIR, such as xenon lamps. In addition, cellular and tissue autofluorescence is lowest in the NIR spectral region [4,26]. In deep-tissue imaging, iRFPs were shown to be superior to the brightest available far-red GFP-like FPs in direct comparison [16,17], due to low autofluorescence in NIR combined with better NIR light penetration and less scattering. Interestingly, the relatively dim and the most red-shifted iRFP720 was found to be the most sensitive probe among FPs for deep-tissue imaging [15,27].

Apparent brightness of NIR FPs in cells, so-called cellular brightness, does not always correlate with molecular brightness [1,25]. It also depends on protein stability and BV binding efficiency. Early NIR FPs, such as IFP1.4 [20], suffered from poor BV incorporation in mammalian cells, leading to their poor brightness (8% for IFP1.4 versus iRFP713 [17]). Screening protein variants in mammalian cells during protein engineering allowed iRFPs to be obtained that do not require an exogenous BV supply and that can be used similarly to GFP-like probes [16,17].

Bright NIR FPs, such as those in the iRFP family, are dimers and may not be suitable for protein tagging and engineering of biosensors as they can interfere with proper localization and function of fused functional molecules by inducing their dimerization. The recent development of bright monomeric NIR FPs [18,19,22] has changed this situation the same way that the development of monomeric mFruits [28] from dimeric DsRed GFP-like FPs did a decade ago. Moreover, with advances in technical approaches, NIR probes can allow deeper *in vivo* imaging at higher resolution than probes available previously. Here, we focus on new possibilities opened by monomeric NIR FPs and biosensors. We provide an overview of the monomeric NIR FPs and their properties, describe uses of NIR probes for multiplexed experiments, discuss the newly designed NIR **Förster resonance energy transfer (FRET)** pair and NIR FRET biosensors, describe NIR reporters based on changes in protein amount and their use across spatial scales, and provide examples where synergistic advancements in probe engineering and development of imaging techniques resulted in resolution as high as subcellular at millimeter depths in tissue.

A Palette of Monomeric NIR FPs

Recently developed monomeric miRFPs have properties similar to dimeric iRFPs (Table 1); however, the monomeric state makes them suitable for a variety of protein fusions. An engineering challenge was involved in developing bright monomeric FPs: simple disruption of the dimeric interface known from the crystal structures results in decreased brightness in mammalian cells, possibly caused by reduced protein stability. The first bright monomeric NIR FPs, that is, mIFP [22] and miRFP670, miRFP703, and miRFP709 [18], were engineered from bacterial phytochromes that do not dimerize via their chromophore-binding domain. Additional mutagenesis on the possible dimerizing interface in miRFPs resulted in FPs that behaved as monomers even at a high concentration of 30 mg/ml. Building on this result and structure studies, dimeric iRFPs were monomerized without a loss of brightness (Figure 1A) [19,29]. These FPs have properties (Table 1) similar to their dimeric counterparts and make a whole iRFP palette available as miRFPs. Importantly, miRFPs inherited high effective cellular brightness of dimeric iRFPs resulting from efficient BV incorporation. Monomeric state enabled a use

Glossary

Adaptive optics (AO): correction of aberrations in scattering tissue to enhance resolution of the optical imaging at depth. A direct wavefront-sensing approach using fluorescence guide stars is a method to correct these aberrations and increase depth of high-resolution imaging.

All-optical electrophysiology: an approach that combines light-induced perturbation (using channelrhodopsins as optogenetic tools) and optical readout (via genetically encoded sensors for membrane voltage or calcium) of neuronal activity.

Bacterial phytochrome photoreceptors (BphPs): multidomain photoreceptors that respond to near-infrared (NIR) light and incorporate the most red-shifted natural chromophore biliverdin (BV). They participate in microbe light-adaptive behavior and activate a biochemical response after light-induced chromophore isomerization and conformational changes in the protein molecule.

Bimolecular fluorescence complementation (BiFC): an approach to study protein–protein interaction based on the reconstruction of a fluorescent protein from split halves fused to the target proteins.

Cellular brightness: effective fluorescence of a NIR FP in a living cell that depends on molecular brightness of the probe, protein expression level, folding efficiency and stability of the probe, and affinity and specificity of the apoprotein to BV chromophore.

Circular permutation: a rearrangement of the order of protein sequence made by connecting the original N and C termini via peptide linkers and introducing the novel protein ends.

c-Jun N-terminal kinase (JNKs): a mitogen-activated serine/threonine protein kinases family that participates in signaling pathways in stress responses, including cytokines, ultraviolet irradiation, heat and osmotic shocks, proliferation, embryonic development, and apoptosis.

Förster radius (Ro): characterizes the theoretical efficiency of Förster resonance energy transfer (FRET)

of miRFPs as versatile fusion tags. It was shown that miRFPs indeed localize well in protein fusions (Figure 1B).

Multiplexed Imaging and Optogenetics with NIR Genetically Encoded Probes

NIR probes complement GFP-like probes for multicolor imaging. Moreover, spectrally distinct m/iRFPs can be used in multicolor imaging (Figure 1C). miRFPs and mIFP allow crosstalk-free multicolor labeling with green and red GFP-like FPs (Figure 1D,E). miRFP703 was used in multicolor imaging in a study of a mechanism of invasion and metastasis in cancer cells associated with activity of Rac3 GTPase localized at invadopodia [30]. Invadopodia, which are plasma membrane protrusions, mediate the degradation of extracellular matrix, promoting cancer cell invasion. Four-color imaging of miRFP703-labeled invadopod core protein cortactin was used to detect mature invadopodia that colocalized with intra- and extracellular-exposed MT1-matrix metalloproteinase responsible for matrix degradation (Figure 1F). Cortactin-miRFP703 was also used to visualize invadopodia simultaneously with the activity of Rac3 biosensor based on the mCerulean-mVenus FRET pair [30]. Dimeric iRFPs can be used for multicolor imaging to highlight a whole cell or an organelle and in protein fusions where their dimeric state does not interfere with functionality (see examples in [31] for multicolor tracing of motor recruitment to cargo and in [32] for use of iRFP713 in adeno-associated virus in mice expressing EGFP and tdTomato).

The NIR spectra of iRFPs make them ideal probes for multiplexing with blue-green optogenetic tools. For example, iRFP713 was used to track nucleus movement to the periphery in muscle cells after optogenetically (with channelrhodopsin ChR2) induced contraction (Figure 1G) [33]. Also, iRFP713 was used to label an engineered blue light-activated calcium channel switch named BACCS [34]. BACCS activation results in calcium-induced gene expression. Changes in the calcium concentration were detected with green Fluo4/AM indicator simultaneously with visualization of NIR iRFP713-BACCS (Figure 1H). Another example is the use of iRFP713-$PH_{PLC\delta1}$ fusion as a biosensor for blue light-induced dephosphorylation of lipid phosphatidylinositol 4,5-bisphosphate via an engineered optogenetic system (Figure 1I) [35]. Optogenetic control of lipid modifications coupled with visualization of these modifications is an example of a powerful all-optical approach to study cell signaling in their native environment. iRFP713 was also used to label optogenetic channelrhodopsins, allowing their visualization without affecting functionality [9]. Although these and other experiments were possible with dimeric iRFPs, the availability of miRFPs should make multiplexed imaging and optogenetics widely applicable, because monomeric miRFPs are versatile protein labels and optimal building blocks for engineering of various biosensors for cell signaling pathways.

Fully NIR FRET Pair and FRET-Based Biosensors

Multispectral monomeric miRFPs allow designing various FRET biosensors. Earlier FRET pair of dimeric iRFP713 combined with mKate2 was suboptimal and applied only to caspase-3 sensor [36]. Possibly, a combination of miRFPs with advanced red fluorescent proteins (RFPs) [37,38] can produce an efficient FRET pair with high dynamic range of response. Recently, a fully NIR FRET pair was reported [19]. Advantages of NIR FRET over RFP-NIR FP FRET are similar to advantages of NIR FPs over RFPs: better spectral separation in multispectral experiments, lower autofluorescence background, less scattering, and better light penetration in tissue for *in vivo* experiments. miRFP670-miRFP720 FRET pair is characterized by good spectral overlap between donor emission and acceptor excitation, minimal direct

between light-emitting donor and light-absorbing acceptor molecules. Ro is the distance at which the energy transfer efficiency is 50%. It depends on the overlap between the donor emission and the acceptor absorbance spectra, fluorescence quantum yield of the donor, molar extinction coefficient of the acceptor, refractive index of the medium, donor emission wavelength, and calculated for freely rotating chromophores.

Förster resonance energy transfer (FRET): a mechanism of non-radiative energy transfer from a donor fluorophore in its electronic excited state to an acceptor fluorophore through dipole–dipole coupling.

Fucci (fluorescence ubiquitination-based cell cycle indicator): a technology that uses a genetically encoded two-color indicator system to analyze cell cycle dynamics within a cell population.

Optogenetics: an approach that uses genetically encoded constructs to precisely and non-invasively manipulate specific molecular process or cell function by light.

Photoacoustic tomography (PAT): an imaging technique that is based on photoacoustic effect and combines optical absorption and acoustic detection. The probe is excited with light but instead of fluorescence, thermoelastically generated acoustic waves are detected. Applied for deep tissue imaging, it enables higher spatial resolution at greater depths than purely optical imaging, because ultrasonic waves are scattered less than photons in tissue.

Protein kinase A (PKA): a cAMP-dependent serine/threonine kinase, a crucial enzyme in cell signaling cascades initiated by G protein-coupled receptors through cAMP second messenger. It participates in several processes, including regulation of glycogen, sugar, lipid metabolism, and activation of reward system in the brain.

Rac1 GTPase: a member of the Rho family of small GTPases that regulates multiple signaling pathways controlling cell motility, proliferation, and differentiation and also glucose uptake. Since it is crucial for lamellipodia formation in cell motility,

cross-excitation of the acceptor among miRFP combinations, and a high **Förster radius (Ro)** of 8.3 nm [19]. For comparison, Ro is 4.9 nm for ECFP-EYFP and 5.4 nm for mCerulean-mVenus [39]. The performance miRFP670-miRFP720 FRET pair was tested in a fusion containing caspase-3 cleavage site. The response of 34% changes in the donor/FRET ratio for miRFP670-miRFP720 is comparable to responses of cyan-yellow CFP-YFP FRET pairs [40,41]. Therefore, this NIR FRET pair can be used to re-design FRET biosensors into the NIR spectral range.

GFP-like FRET biosensors for key molecules in cell signaling, including Ca^{2+}, cAMP, phospholipids, small GTPases, and protein kinases, are widely used in studies of signaling cascades. NIR FRET biosensors for these molecules are in high demand and will be engineered in the near future. By exchanging GFP-like FPs for miRFPs in kinase sensors [42], NIR biosensors for **protein kinase A (PKA)** AKAR and **c-Jun N-terminal kinases (JNKs)** JNKAR were obtained (Figure 2A–C). Further optimization by changing the length and composition of the linkers can improve the response of the sensors, as was performed for the NIR biosensor for **Rac1 GTPase**, which regulates signaling pathways controlling cell motility [43] (Figure 2D) [19]. The resulting Rac1 biosensor is a robust probe with a high dynamic range of response (up to 2.7-fold changes in FRET/donor ratio). The NIR Rac1 sensor can be combined with CFP-YFP biosensors and blue-green optogenetic tools. Simultaneous imaging of Rac1 in NIR and other GTPases in the visible range enables the direct visualization of spatiotemporal coordination of GTPase activities at the cell leading edge that leads to protrusion-retraction cycles and stalling of the edge. By imaging of NIR Rac1 and CFP-YFP RhoA biosensors, the antagonism between activities of these two GTPases was directly characterized in the same cell, for the first time (Figure 2E). Spatiotemporal coordination of Rac1 activity by its negative regulator guanosine nucleotide dissociation inhibitor (GDI) was revealed by simultaneous imaging of NIR Rac1 and CFP-YFP Rac1-GDI binding sensor. Furthermore, this biosensor was used simultaneously with optogenetic activation of the Rac1 GTPase by the LOV-TRAP tool.

NIR Reporters for Imaging across Scales

A toolbox of NIR FRET and intensiometric biosensors based on conformational changes in the protein backbone upon activation is yet to be developed. NIR reporters based on changes in the amount of fluorescent tag because of its synthesis/degradation or reconstitution are already available and have been applied to imaging at different spatial scales.

The reporter for canonical activation of the nuclear factor-κB (NF-κB) pathway is a fusion of miRFP703 with inhibitor of NF-κB (IκBα), which binds NF-κB transcription factor and keeps it in the cytoplasm [18]. This pathway is associated with immune response, cellular proliferation, and apoptosis [44]. Upon its activation, IκBα is degraded together with miRFP703 and a decrease of fluorescence can be detected (Figure 3A). This reporter was visualized in cells upon addition of tumor necrosis factor-α (Figure 3B) and in animals upon injection of lipopolysaccharide, triggering inflammation (Figure 3C).

The NIR cell cycle reporter [18] is based on **Fucci** technology [45] that consists of two spectrally distinguishable miRFP670 and miRFP709 fused to the fragments of Geminin and Cdt1. The levels of these proteins participating in the licensing of replication origins change reciprocally (Figure 3D). Using this reporter, dividing cells were distinguished from non-dividing cells in culture (Figure 3E) and implanted in mice (Figure 3F) by detecting fluorescence in two channels corresponding to miRFP670 and miRFP709. A similar cell cycle reporter was developed using a pair consisting of IFP2.0 and smURFP [24].

it is involved in cell invasion and metastasis in cancer.

Structured illumination microscopy (SIM): a widefield technique that relies on a grid pattern in one of the illumination apertures to extract information from the image focal plane and produce an approximately twofold increase in resolution in two or three dimensions.

Two-photon (2P) microscopy: a microscopy technique based on two-photon excitation of fluorescence (two long-wavelength, low-energy photons cause higher energy electronic transition in a fluorescent molecule). Confined focal volume and deeper penetrating NIR light result in cellular resolution up to 1 mm depth in tissue.

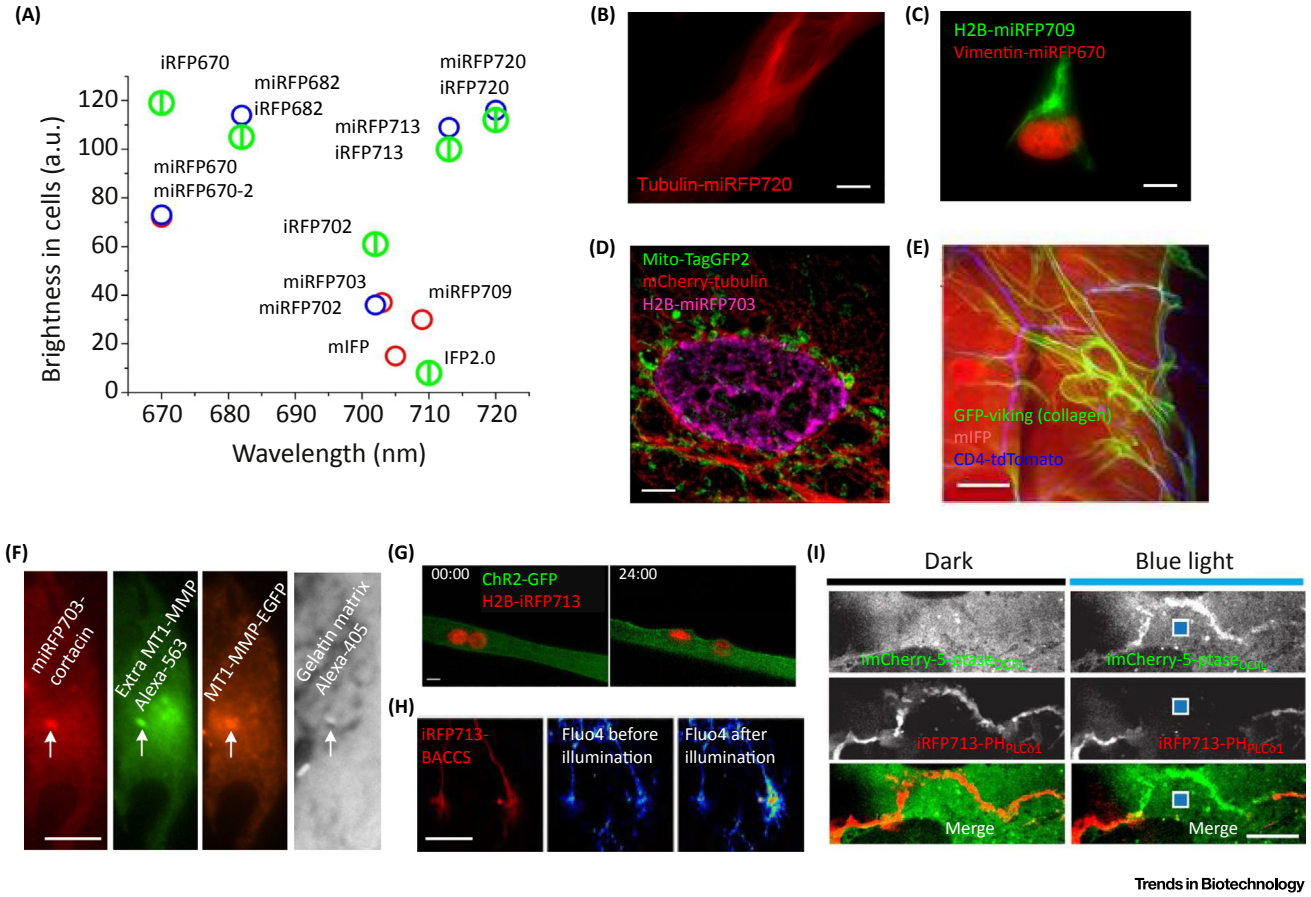

Figure 1. NIR FPs and Their Applications in Multiplexed Imaging and Optogenetics. (A) Effective cellular brightness and emission wavelength maxima of near-infrared (NIR) fluorescent proteins (FPs). Early miRFPs and mIFP are shown as red circles, new miRFPs as blue circles, and dimeric iRFPs as larger green split circles. (B) Tubulin-miRFP720 localizes well in live HeLa cells. Adapted, with permission, from [19]. (C) miRFP670 and miRFP709 allow two-color labeling as shown by simultaneous visualization of H2B and vimentin in HeLa cells. (D,E) miRFPs and mIFP allow crosstalk-free three-color imaging together with green and red GFP-like FPs as shown by structured illumination microscopy in HeLa cells (D) and by visualization of abdomen muscle (mIFP), class IV dopaminergic neurons (CD4-tdTomato), and extracellular collagen matrix (GFP) in *Drosophila* (E). (C,D) Adapted from [18] under the Creative Commons Attribution license; (E) adapted, with permission, from [22]. (F) miRFPs was used in four-color imaging to localize invadopod (marked by white arrow, miRFP703), colocalized with intracellular (EGFP) and extracellular (Alexa-565) MT1-matrix metalloproteinase (MMP), and matrix degradation (Alexa-405). Courtesy of Louis Hodgson. (G–I) iRFP713 was used with blue light-induced optogenetic tools, including chanelrhodopsin ChR2 in muscle {(G) adapted, with permission, from [33]}, channel switch BACCS in neurons {(H) adapted under the Creative Commons Attribution license from [34]}, and system CRY2/CIBN for recruitment of inositol-5-phosphatase (5-ptase) to the cell membrane in COS-7 cells (I, adapted, with permission, from [35]). Scale bars, 5 μm in (D,I); 10 μm in (B,C,G); 20 μm in (E,F); and 50 μm in (H).

NIR reporters for protein–protein interactions are based on **bimolecular fluorescence complementation (BiFC)** of the two split fragments: the PAS and the GAF domains of NIR FPs (Figure 3G) [46–49]. An iSplit reporter based on iRFP713 was successfully applied in mammalian cells (Figure 3H) and in mice (Figure 3I) [47]. New monomeric versions miSplit709 and miSplit670 have severalfold lower background and higher contrast than iSplit [18]. BiFC contrast decreases if split fragments tend to self-associate. BiFC contrast in cultured cells for miSplits was found to be 18-fold for miSplit709 and 41-fold for miSplit670 [18]. For comparison, the highest reported contrast for BiFC derived from GFP-like Venus in similar conditions was 17-fold [50]. miSplit670 and miSplit709 share the same PAS domain but differ in their GAF

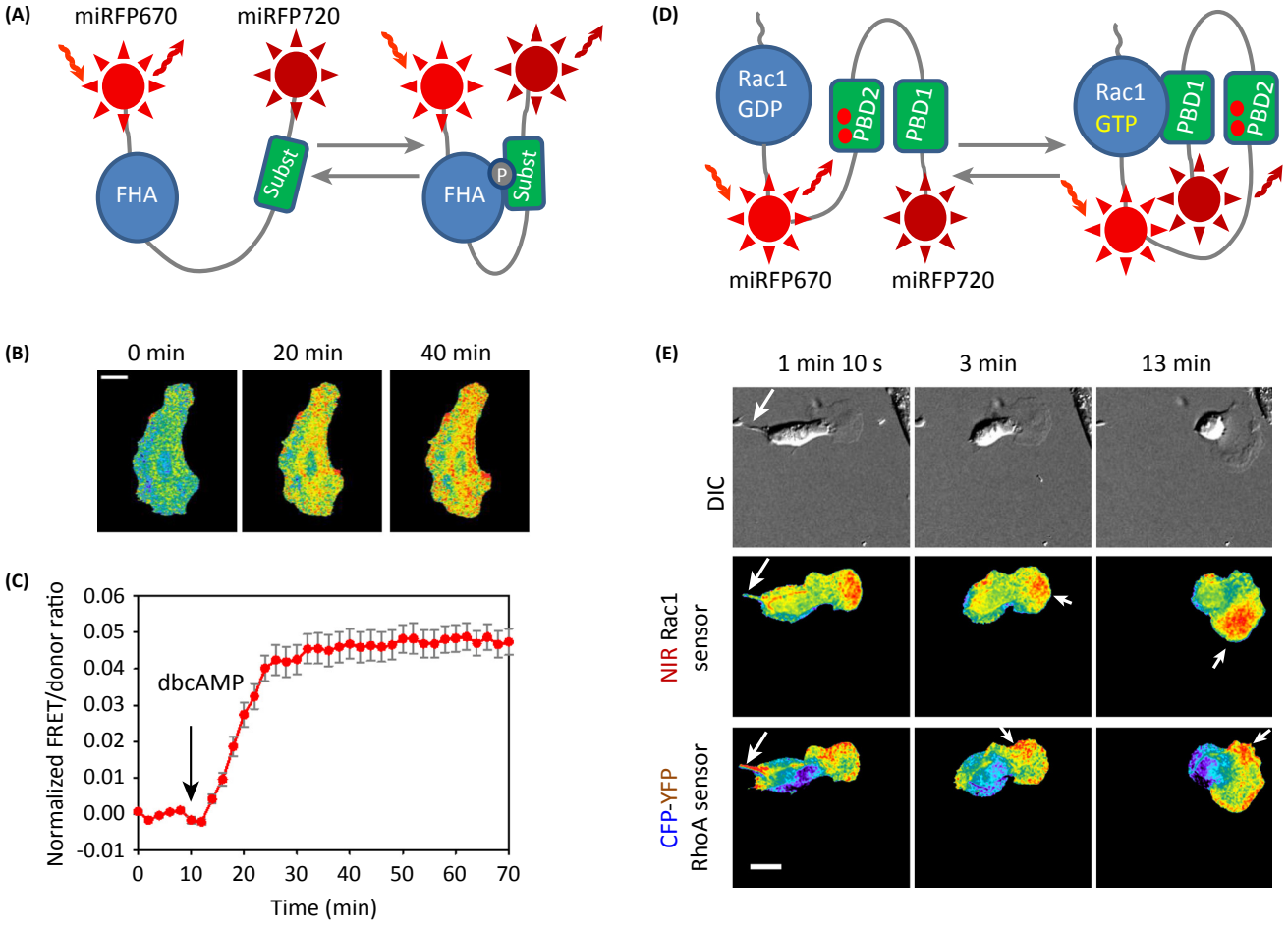

Figure 2. Single-Chain NIR Biosensors for Different Targets in Signaling Cascades Based on miRFP670-miRFP720 FRET Pair. (A) Schematics of the NIR FRET AKAR biosensor for PKA and JNKAR biosensor for JNK kinases. FHA is the phosphopeptide binding domain that recognizes phosphorylated peptide marked as subst. (B,C) NIR AKAR PKA kinase biosensor was validated in live HeLa cells stimulated with 1 mM dibutyryl cAMP (dbcAMP); time-lapse images (B) and the corresponding plot (C) are shown. (D) Schematics of the FRET Rac1 biosensor. PBD1 is a p21-binding domain 1, PBD2 is a mutant p21-binding domain. Rac1 is a full-length Rac1 post-translationally isoprenylated for membrane localization. (E) Combination of NIR and cyan-yellow FRET biosensors for simultaneous imaging of Rac1 and RhoA activities in an MEF/3T3 cell. DIC, differential interference contrast. Rac1 is predominantly localized at the leading edge, whereas RhoA activity is mostly localized at the retracting tail, the side edges, and at the back of the leading-edge protrusions (see arrows). (B,E) FRET/donor ratio is shown in pseudocolor. Scale bar, 20 μm. (C) Mean ± SEM ($n = 3$) of the FRET/donor ratio for the whole cell plotted versus time. (B,C,E) Adapted, with permission, from [19].

domains, specifically, amino acids near the chromophore in the GAF domains that define spectral properties. Thus, the combination of miSplit670 and miSplit709 can be adapted for detection of interaction of the protein fused to the PAS domain with two alternative binding partners fused to the $mGAF_{670}$ or $mGAF_{709}$ domains by the wavelength of the reconstituted fluorescence [18]. miSplits were also applied to RNA labeling. Fused to two high-affinity bacteriophage RNA-binding proteins MCP and PCP, miSplits reconstituted fluorescence when bound to mRNA molecules tagged with 12 repeats of corresponding RNA-binding sites (MBS and PBS). Since self-assembly for miSplits and the autofluorescence background are low, this techniques provides a sensitive method for RNA detection.

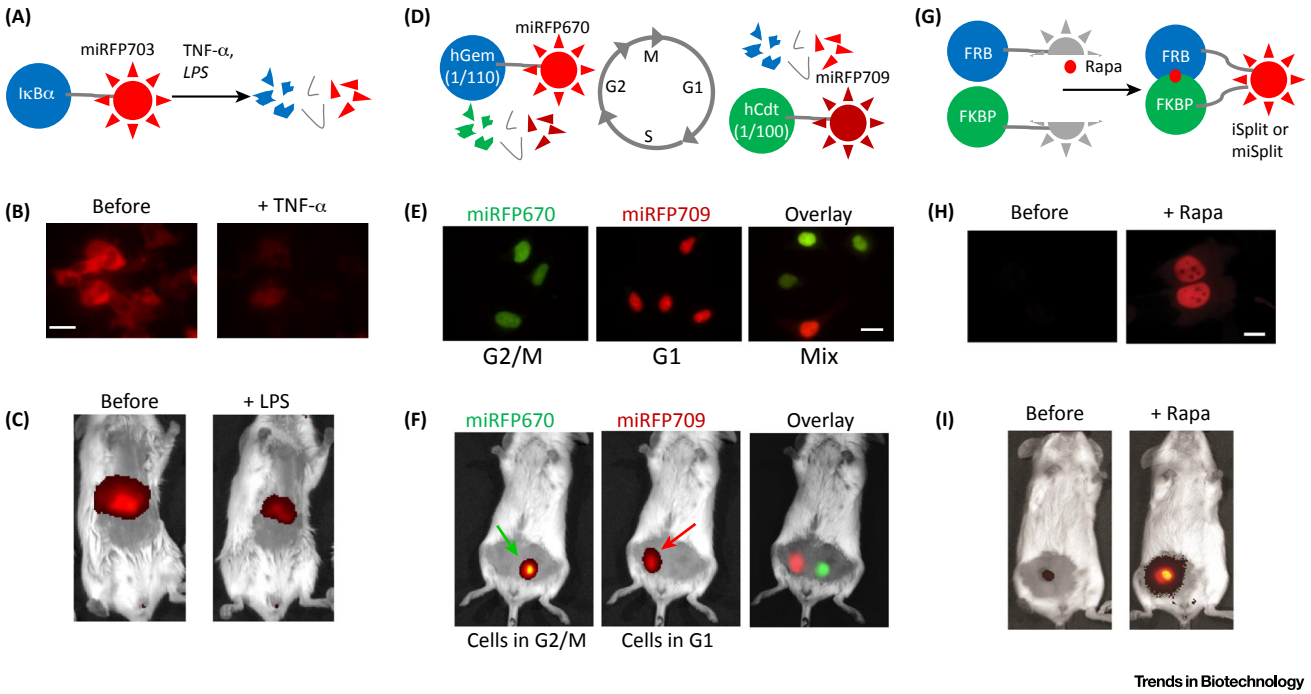

Figure 3. Multiscale Imaging of NIR Reporters. (A) Schematics of the inhibitor of nuclear factor-κB (IκBα)-miRFP703 reporter for canonical activation of nuclear factor-κB pathway. Its activation by tumor necrosis factor α (TNF-α) or lipopolysaccharide (LPS) results in IκBa degradation together with miRFP703. (B,C) Visualization of IκBa-miRFP703 reporter in human embryonic kidney 293 cells (B) and in a mouse liver (C). (B,C) Adapted under the Creative Commons Attribution license from [18]. (D) Schematics of the NIR cell cycle reporter. miRFP670-hGem(1/110) and miRFP709-hCdt1(1/100) are reciprocally produced and degraded in a cell cycle-dependent manner. (E,F) Visualization of NIR cell cycle reporter in synchronized (in G2/M and G1 phases) and non-synchronized (mix) HeLa cells (E) and in a mouse with implanted cells (F). (E,F) Adapted under the Creative Commons Attribution license from [18]. (G) Schematics of the NIR bimolecular fluorescence complementation reporters iSplit and miSplits. Two split fragments (the PAS and the GAF domains of iRFP or miRFP) are not fluorescent as separate polypeptides until two fusion proteins interact. Here, FRB and FKBP interact in the presence of rapamycin (rapa). (H,I) Visualization of iSplit reporter in HeLa cells (H) and in a mouse xenograft tumor (I). (H,I) Adapted, with permission, from [47].

Circular permutation of IFP proteins was used to make a fluorogenic reporter for protease activity, including iCasper applied to image apoptosis during morphogenesis and tumorigenesis in *Drosophila* [51]. This reporter is based on cleavage-dependent chromophore incorporation.

Scaling down in spatial resolution, miRFPs and mIFP probes were applied to sub-diffraction **structured illumination microscopy (SIM)** (Figure 1D) [18,22]. Furthermore, NIR FPs were used in recent two-wavelength total internal reflection fluorescence microscopy simultaneous two-wavelength axial ratiometry with 20-nm axial resolution [52]. Using this method, endocytosis of EGFR labeled with both EGFP and iRFP713 was visualized in real time.

Imaging of NIR Probes *In Vivo* with Enhanced Resolution

Light scattering, aberrations, tissue absorbance, and autofluorescence are major obstacles for *in vivo* imaging. Deep penetration of NIR light in tissue and low autofluorescence in NIR make NIR FPs suitable for sensitive imaging *in vivo* (Table 2). However, the resolution is poor due to light scattering, which is reduced in NIR but still present, and optical aberrations. In this section, we discuss recent imaging techniques that use NIR probes to obtain higher resolution at larger depths.

Table 2. Methods for Imaging of NIR Probes across Spatial Scales

Method	Probe	Spatial resolution	Temporal resolution	Sensitivity	Spectral multiplexing	Refs
Animal whole-body, deep tissue, and organ imaging						
Planar fluorescence imaging	iRFPs, miRFP, NIR biosensors	>1 mm up to 2 cm deep	≥1 ms time resolution[a]	$\geq 10^5$ cells up to 2 cm deep	Two-color imaging with m/iRFP670 and m/iRFP720; combination with blue light optogenetic tools	[1,15,17]
Fluorescence tomography		>1 mm up to 2 cm deep	≤1 s time resolution[a]			[2,59]
Planar NIR bio-luminescence imaging	iRFPs–RLuc8s	>1 mm up to 2 cm deep	≥1 ms time resolution[b]	$>10^4$ cells up to 2 cm deep		[75]
Fluorescence lifetime tomography	iRFPs, miRFP, NIR biosensors	~1 mm up to 1 cm deep	≤1 s time resolution[a]	$\sim 10^4$ cells up to 1 cm deep		[76]
Photoacoustic tomography		<1 mm up to 1 cm deep	<1 s time resolution[a]	$>10^4$ cells up to 1 cm deep		[57–59,77]
Reversibly-switchable photoacoustic tomography	BphP1	≥100 μm up to 1 cm deep	>1 s time resolution	$>10^2$ cells up to 1 cm deep	Combination with blue light optogenetic tools	[60,78]
In vivo cellular and subcellular imaging						
2P microscopy	iRFPs, miRFP, NIR biosensors	10 μm up to 1 mm deep	>1 ms time resolution[a]	1 cell up to 1 mm deep	Combination with blue light optogenetic tools	[10,55]
2P microscopy with AO		>1 μm up to 1 mm deep		Subcellular up to 1 mm deep		[56]
Ex vivo cell analysis						
Flow cytometry	miRFPs, iRFPs	Individual cells	–	Individual cells	≤4 multispectral m/iRFPs and several dyes/ GFP-like FPs	[17,79]
Cells and subcellular structures						
Fluorescence microscopy (wide-field and confocal)	iRFPs, miRFP, NIR biosensors	≥350 nm	≥1 ms time resolution[a]	Molecules[a]	Crosstalk-free imaging with green and red GFP-like FPs; multicolor imaging; combination with blue light optogenetic tools	[18,19,22]
SIM		≥175 nm	>1 ms time resolution[a]	Subcellular structures		[18,22]

[a]Depends on the power of light source and sensitivity of the detector/camera.
[b]Depends on camera sensitivity.

Two-photon (2P) microscopy is traditionally used for cellular and subcellular resolution *in vivo* imaging, especially in neuroscience [53]. Some properties of iRFPs in 2P microscopy have recently been characterized [10]. For example, a standard Ti-Sapphire laser excites iRFPs at 880 nm more effectively than the laser equipped with optical parametric oscillator at 1280 nm (Figure 4A). Thus, iRFPs are suitable for single-wavelength 2P imaging together with EGFP/EYFP at 880 nm (Figure 4B). Further improvement of resolution at tissues located at depths up to 1.6 mm can be achieved by using a combination of **adaptive optics (AO)** with 2P microscopy [54,55]. The reduced scattering of NIR fluorescence promoted the use of iRFPs

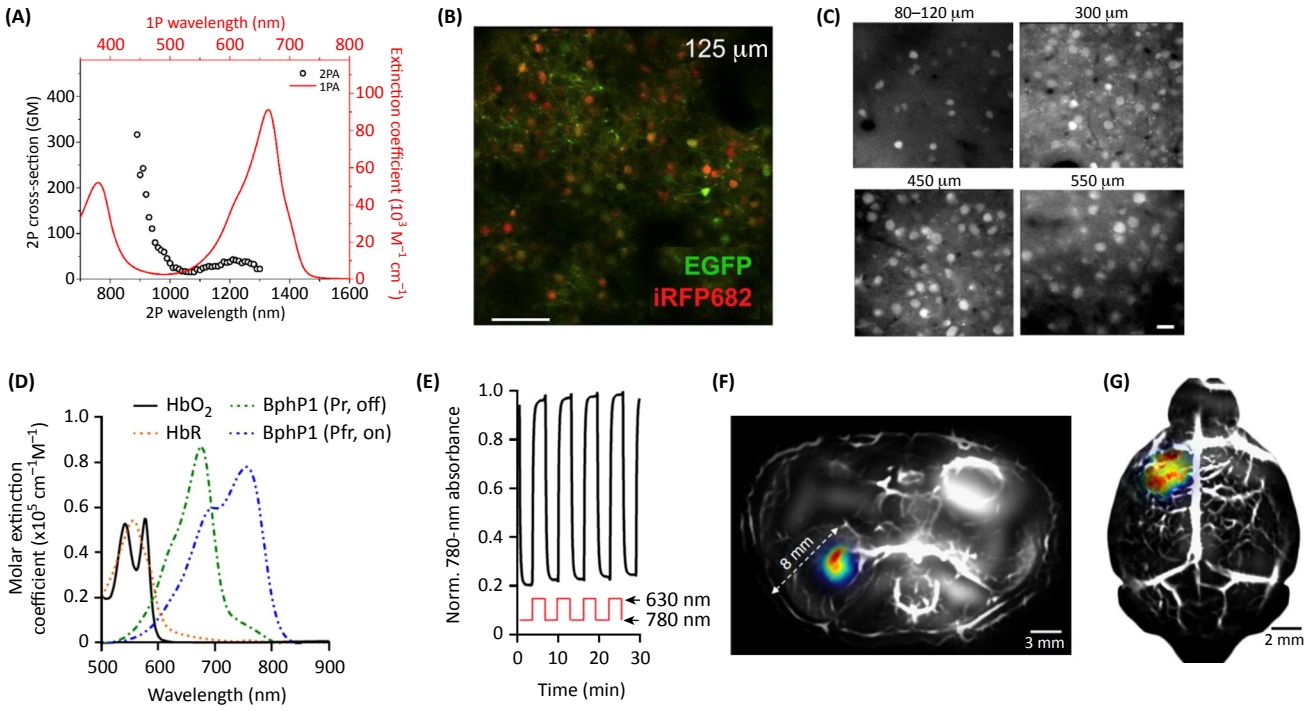

Figure 4. High-Resolution *In Vivo* Imaging of NIR Probes. (A) iRFPs can be effectively excited by Ti-Sapphire laser at 880 nm as shown by two-photon (2P) absorption spectra of iRFP682 (open circles). One-photon (1P) absorption spectra of iRFP682 is also shown (unbroken line). (B) Visualization of iRFP682 and EGFP in neurons of mouse cortex layer 2/3 using *in vivo* single-wavelength (880-nm) 2P microscopy. (A,B) Adapted, with permission, from [10]. (C) Visualization of iRFP713 in neurons of mouse cortex layers 1, 2/3, 4, and 5 using 2P microscopy with adaptive optics wavefront correction. (C) Adapted, with permission, from [9] and [56]. (D) Photoacoustic tomography of bacterial phytochrome BphP1 Pfr (marked as ON) and BphP1 Pr (marked as OFF) allows to subtract background absorption by hemoglobin (HbO_2) and deoxyhemoglobin (HbR). (E) BphP1 can be repeatedly photoswitched by 780- and 630-nm light between its Pfr ON state and Pr OFF state. Norm., normalized. (F,G) Reversibly switchable photoacoustic computed tomography of deep-seated tumors *in vivo*; this technique can visualize kidney (F) and brain (G) tumors and vasculature as overlays of the ON state image (BphP1, pseudocolor) and the OFF state image (hemoglobin, gray) with exceptionally high resolution. (F,G) Adapted, with permission, from [60]. Scale bars, 100 μm in (B) and 20 μm in (C).

as guide stars for correcting aberrations by applying a direct wavefront sensing method [56]. Using this technique, iRFP713 optical guide star and green calcium biosensor GCaMP6 were imaged in the primary visual cortex of a mouse at a depth of 550 μm (Figure 4C).

Another approach to overcome the problem of light scattering *in vivo* is **photoacoustic tomography (PAT)**. iRFPs are genetically encoded probes of choice for PAT because their absorption is well differentiated from that of hemoglobin in blood. Their exceptional performance in PAT to visualize deep-seated tumors with submillimeter resolution at up to 8 mm in depth has been extensively used [57–59]. A recent approach, called reversibly switchable photoacoustic computed tomography, enabled even deeper imaging at higher resolution: 100 μm at depths up to 10 mm [60]. This technique relies on the reversibly photoswitchable bacterial phytochrome BphP1, which is a precursor of miRFPs (Figure 4D,E), and uses differential photoacoustic imaging to cancel nonspecific light absorption by tissue. Using this technique, small deep-seated tumors that were undetectable with traditional PAT in the kidney and in the brain were visualized (Figure 4F,G).

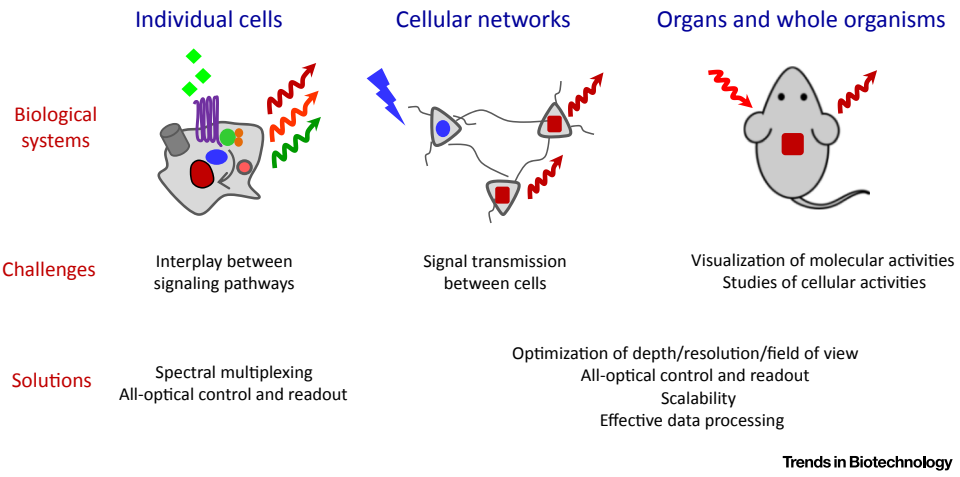

Figure 5. Optical Technologies Aided by NIR Probes to Address Current Challenges. Challenging studies at different spatial scales from cells to cellular networks to organs and whole organisms (see 'Biological Systems' section) are presented (see 'Challenges' section). Corresponding optical technologies that rely on near-infrared (NIR) fluorescent probes and NIR biosensors and could address the challenges are listed (see 'Solutions' section).

Concluding Remarks and Future Perspectives

The recent development of monomeric NIR FPs, reporters, and biosensors, allows direct monitoring of active processes in multiplexed experiments at different spatial scales (Table 2). Combined with advanced imaging technologies, such as 2P microscopy with AO, and PAT, they should help to mitigate the current trade-off between imaging depth, spatial resolution, and field of view (Figure 5).

The brightest NIR FPs (Table 1), such as iRFPs and miRFPs, are sufficiently optimized and can be used as easily as GFP-like FPs. NIR FPs have low cytotoxicity and high photostability, but their fluorescence quantum yield can be improved (see Outstanding Questions). Future protein engineering efforts may address this challenge by using structure insights [61,62], novel precursor bacterial phytochromes for evolution, and advanced screening approaches, such as using fluorescence lifetime that is insensitive to expression level of fluorescent probe and thus allows for selection of bacteria expressing the intrinsically bright probes [63]. Another challenge is to shift spectra of FPs further in the NIR region to allow deeper light penetration in tissue, lower autofluorescence background, and thus higher imaging sensitivity. Attempts to shift the spectra by stabilizing the Pfr state of phytochromes absorbing at ~740 nm have not been successful so far.

The NIR Rac1 biosensor should inspire the generation of more NIR biosensors for a wide variety of cell signaling activities based on NIR FRET technology. The activities of interest include tyrosine and serine-threonine kinases; small GTPases; and second messengers including calcium, cAMP, and lipid-derived signaling molecules. Compatible with GFP-like probes and optogenetic tools, NIR biosensors should allow studies that are currently challenging, such as visualizing multiple events in signaling pathways and detecting interplay between pathways, studying signal transmission between cells, and performing visualization and causal studies of molecular and cellular activities *in vivo* (Figure 5).

Together with blue-green optogenetic tools, NIR biosensors should enable crosstalk-free, precise, and patterned manipulation of cellular functions and simultaneous detection of

Outstanding Questions

Is it possible to engineer NIR FPs with increased quantum yield? What is the best strategy for directed molecular evolution to achieve this goal?

How can NIR FPs with emission maxima above 720 nm be engineered? Is it possible to do this by stabilizing the Pfr state of bacterial phytochromes?

When will NIR FRET biosensors for functional molecules in cell signaling cascades, such as protein kinases, phosphatases, GTPases, and second messengers, be developed? Will the miRFP670-miRFP720 FRET pair be suitable for re-engineering available GFP-like FRET sensors into NIR? How will NIR FRET biosensors perform compared with the original GFP-like probes?

When will NIR biosensors for calcium and voltage changes be developed to allow straightforward all-optical electrophysiology for causal studies with precise spatiotemporal resolution? How will they perform compared with available GFP-like biosensors?

Can NIR single-color intensiometric biosensors be generated using NIR FP scaffold? What is the best strategy to achieve this: circular permutation or insertion of sensing domains into unperturbed NIR FPs?

Is it possible to improve resolution and/or sensitivity in *in vivo* imaging with NIR FPs?

When will transgenic mouse models expressing NIR FPs and biosensors be available for a wide community of researchers and companies focused on preclinical studies?

molecular activities. Such all-optical control and readout can involve optogenetic tools to interrogate signaling cascades, starting from receptor activation and ending with gene transcription and genome editing (reviewed in [64,65]). NIR biosensors for calcium and membrane voltage changes are highly desired for combination with channelrhodopsins to allow **all-optical electrophysiology** [66]. Although this approach was applied to study neuronal circuits [67] and cardiac dynamics [68], crosstalk between tools, low brightness of current red-shifted biosensors, and a need for a specialized experimental setup prevent its wide use in research community.

We also anticipate future engineering of intensiometric biosensors based on modulation of fluorescence of a single NIR FP. Whereas FRET biosensors allow quantitative readouts and efficient segregation of their signal from hemodynamic signal components, intensiometric biosensors may provide higher dynamic ranges of response and require only a single bandwidth for imaging. These biosensors can be developed by engineering circularly permuted monomeric NIR FPs fused to sensing domains or by using FPs with insertions containing sensing domains that reversibly modulate fluorescence upon ligand binding [69].

The applicability of NIR biosensors to imaging at different spatial scales, from subcellular to organismal, should facilitate workflows in drug screening from cells to whole animals and stimulate the development of novel models of diseases. Several transgenic animals have been developed using iRFPs (*Drosophila* [22,70], mice [71], and rats [9]). We expect transgenic mice expressing NIR biosensors to be generated in the near future. These mouse models should advance preclinical studies by facilitating drug screening and validation *in vivo*.

Acknowledgments

This work was supported by grants GM122567 and NS103573 from the National Institutes of Health, ERC-2013-ADG-340233 from the EU 7th Framework Programme, 16-04-01515 from the Russian Foundation for Basic Research, and a grant from the Molecular and Cell Biology Program of the Russian Academy of Sciences. We apologize to researchers whose work we could not quote here due to space limitation and the focus of this review article.

References

1. Shcherbakova, D.M. *et al.* (2015) Near-infrared fluorescent proteins engineered from bacterial phytochromes. *Curr. Opin. Chem. Biol.* 27, 52–63
2. Lu, Y. *et al.* (2013) *In vivo* imaging of orthotopic prostate cancer with far-red gene reporter fluorescence tomography and *in vivo* and *ex vivo* validation. *J. Biomed. Opt.* 18, 101305
3. Jiguet-Jiglaire, C. *et al.* (2014) Noninvasive near-infrared fluorescent protein-based imaging of tumor progression and metastases in deep organs and intraosseous tissues. *J. Biomed. Opt.* 19, 16019
4. Hock, A.K. *et al.* (2014) iRFP is a sensitive marker for cell number and tumor growth in high-throughput systems. *Cell Cycle* 13, 220–226
5. Lai, C.W. *et al.* (2016) Using dual fluorescence reporting genes to establish an *in vivo* imaging model of orthotopic lung adenocarcinoma in mice. *Mol. Imaging Biol.* 18, 849–859
6. Genevois, C. *et al.* (2016) *In vivo* follow-up of brain tumor growth via bioluminescence imaging and fluorescence tomography. *Int. J. Mol. Sci.* 17, 1815
7. Chao, C.N. *et al.* (2018) Gene therapy for human glioblastoma using neurotropic JC virus-like particles as a gene delivery vector. *Sci. Rep.* 8, 2213
8. Fyk-Kolodziej, B. *et al.* (2014) Marking cells with infrared fluorescent proteins to preserve photoresponsiveness in the retina. *Biotechniques* 57, 245–253
9. Richie, C.T. *et al.* (2017) Near-infrared fluorescent protein iRFP713 as a reporter protein for optogenetic vectors, a transgenic Cre-reporter rat, and other neuronal studies. *J. Neurosci. Methods* 284, 1–14
10. Piatkevich, K.D. *et al.* (2017) Near-infrared fluorescent proteins engineered from bacterial phytochromes in neuroimaging. *Biophys. J.* 113, 2299–2309
11. Wang, Y. *et al.* (2014) Assessing *in vitro* stem-cell function and tracking engraftment of stem cells in ischaemic hearts by using novel iRFP gene labelling. *J. Cell Mol. Med.* 18, 1889–1894
12. Mezzanotte, L. *et al.* (2017) Optimized longitudinal monitoring of stem cell grafts in mouse brain using a novel bioluminescent/near infrared fluorescent fusion reporter. *Cell Transplant.* 26, 1878–1889
13. Bantounas, I. *et al.* (2018) Generation of functioning nephrons by implanting human pluripotent stem cell-derived kidney progenitors. *Stem Cell Rep.* 10, 766–779
14. Calvo-Alvarez, E. *et al.* (2015) Infrared fluorescent imaging as a potent tool for *in vitro*, *ex vivo* and *in vivo* models of visceral leishmaniasis. *PLoS Negl. Trop. Dis.* 9, e0003666
15. Isomura, M. *et al.* (2017) Near-infrared fluorescent protein iRFP720 is optimal for *in vivo* fluorescence imaging of rabies virus infection. *J. Gen. Virol.* 98, 2689–2698
16. Filonov, G.S. *et al.* (2011) Bright and stable near-infrared fluorescent protein for *in vivo* imaging. *Nat. Biotechnol.* 29, 757–761
17. Shcherbakova, D.M. and Verkhusha, V.V. (2013) Near-infrared fluorescent proteins for multicolor *in vivo* imaging. *Nat. Methods* 10, 751–754

18. Shcherbakova, D.M. *et al.* (2016) Bright monomeric near-infrared fluorescent proteins as tags and biosensors for multiscale imaging. *Nat. Commun.* 7, 12405
19. Shcherbakova, D.M. *et al.* (2018) Direct multiplex imaging and optogenetics of Rho GTPases enabled by near-infrared FRET. *Nat. Chem. Biol.* 14, 591–600
20. Shu, X. *et al.* (2009) Mammalian expression of infrared fluorescent proteins engineered from a bacterial phytochrome. *Science* 324, 804–807
21. Yu, D. *et al.* (2014) An improved monomeric infrared fluorescent protein for neuronal and tumour brain imaging. *Nat. Commun.* 5, 3626
22. Yu, D. *et al.* (2015) A naturally monomeric infrared fluorescent protein for protein labeling *in vivo*. *Nat. Methods* 12, 763–765
23. Auldridge, M.E. *et al.* (2012) Structure-guided engineering enhances a phytochrome-based infrared fluorescent protein. *J. Biol. Chem.* 287, 7000–7009
24. Rodriguez, E.A. *et al.* (2016) A far-red fluorescent protein evolved from a cyanobacterial phycobiliprotein. *Nat. Methods* 13, 763–769
25. Shemetov, A.A. *et al.* (2017) How to increase brightness of near-infrared fluorescent proteins in mammalian cells. *Cell Chem. Biol.* 24, 758-766 e3
26. Lecoq, J. and Schnitzer, M.J. (2011) An infrared fluorescent protein for deeper imaging. *Nat. Biotechnol.* 29, 715–716
27. Luker, K.E. *et al.* (2015) Comparative study reveals better far-red fluorescent protein for whole body imaging. *Sci. Rep.* 5, 10332
28. Shaner, N.C. *et al.* (2004) Improved monomeric red, orange and yellow fluorescent proteins derived from *Discosoma* sp. red fluorescent protein. *Nat. Biotechnol.* 22, 1567–1572
29. Verkhusha, V.V. et al., Albert Einstein College of Medicine, Inc., Monomeric near-infrared fluorescent proteins engineered from bacterial phytochromes and methods for making same, 20180044383
30. Donnelly, S.K. *et al.* (2017) Rac3 regulates breast cancer invasion and metastasis by controlling adhesion and matrix degradation. *J. Cell Biol.* 216, 4331–4349
31. Janssen, A.F.J. *et al.* (2017) Myosin-V induces cargo immobilization and clustering at the axon initial segment. *Front. Cell. Neurosci.* 11, 260
32. Weinhard, L. *et al.* (2018) Microglia remodel synapses by presynaptic trogocytosis and spine head filopodia induction. *Nat. Commun.* 9, 1228
33. Roman, W. *et al.* (2017) Myofibril contraction and crosslinking drive nuclear movement to the periphery of skeletal muscle. *Nat. Cell Biol.* 19, 1189–1201
34. Ishii, T. *et al.* (2015) Light generation of intracellular Ca(2+) signals by a genetically encoded protein BACCS. *Nat. Commun.* 6, 8021
35. Idevall-Hagren, O. *et al.* (2012) Optogenetic control of phosphoinositide metabolism. *Proc. Natl. Acad. Sci. U. S. A.* 109, E2316–E2323
36. Zlobovskaya, O.A. *et al.* (2016) Genetically encoded far-red fluorescent sensors for caspase-3 activity. *Biotechniques* 60, 62–68
37. Shemiakina, I.I. *et al.* (2012) A monomeric red fluorescent protein with low cytotoxicity. *Nat. Commun.* 3, 1204
38. Bindels, D.S. *et al.* (2017) mScarlet: a bright monomeric red fluorescent protein for cellular imaging. *Nat. Methods* 14, 53–56
39. Muller, S.M. *et al.* (2013) Quantification of Förster resonance energy transfer by monitoring sensitized emission in living plant cells. *Front. Plant Sci.* 4, 413
40. Galperin, E. *et al.* (2004) Three-chromophore FRET microscopy to analyze multiprotein interactions in living cells. *Nat. Methods* 1, 209–217
41. Subach, O.M. *et al.* (2008) Conversion of red fluorescent protein into a bright blue probe. *Chem. Biol.* 15, 1116–1124
42. Komatsu, N. *et al.* (2011) Development of an optimized backbone of FRET biosensors for kinases and GTPases. *Mol. Biol. Cell* 22, 4647–4656
43. Bosco, E.E. *et al.* (2009) Rac1 GTPase: a "Rac" of all trades. *Cell. Mol. Life Sci.* 66, 370–374
44. Oeckinghaus, A. and Ghosh, S. (2009) The NF-kappaB family of transcription factors and its regulation. *Cold Spring Harb. Perspect. Biol.* 1, a000034
45. Sakaue-Sawano, A. *et al.* (2008) Visualizing spatiotemporal dynamics of multicellular cell-cycle progression. *Cell* 132, 487–498
46. Tchekanda, E. *et al.* (2014) An infrared reporter to detect spatiotemporal dynamics of protein-protein interactions. *Nat. Methods* 11, 641–644
47. Filonov, G.S. and Verkhusha, V.V. (2013) A near-infrared BiFC reporter for *in vivo* imaging of protein-protein interactions. *Chem. Biol.* 20, 1078–1086
48. Pandey, N. *et al.* (2015) Combining random gene fission and rational gene fusion to discover near-infrared fluorescent protein fragments that report on protein-protein interactions. *ACS Synth. Biol.* 4, 615–624
49. Chen, M. *et al.* (2015) Novel near-infrared BiFC systems from a bacterial phytochrome for imaging protein interactions and drug evaluation under physiological conditions. *Biomaterials* 48, 97–107
50. Kodama, Y. and Hu, C.D. (2010) An improved bimolecular fluorescence complementation assay with a high signal-to-noise ratio. *Biotechniques* 49, 793–805
51. To, T.L. *et al.* (2015) Rationally designed fluorogenic protease reporter visualizes spatiotemporal dynamics of apoptosis *in vivo*. *Proc. Natl. Acad. Sci. U. S. A.* 112, 3338–3343
52. Stabley, D.R. *et al.* (2015) Real-time fluorescence imaging with 20 nm axial resolution. *Nat. Commun.* 6, 8307
53. Svoboda, K. and Yasuda, R. (2006) Principles of two-photon excitation microscopy and its applications to neuroscience. *Neuron* 50, 823–839
54. Ji, N. *et al.* (2008) Advances in the speed and resolution of light microscopy. *Curr. Opin. Neurobiol.* 18, 605–616
55. Kobat, D. *et al.* (2011) *In vivo* two-photon microscopy to 1.6-mm depth in mouse cortex. *J. Biomed. Opt.* 16, 106014
56. Wang, K. *et al.* (2015) Direct wavefront sensing for high-resolution *in vivo* imaging in scattering tissue. *Nat. Commun.* 6, 7276
57. Filonov, G.S. *et al.* (2012) Deep-tissue photoacoustic tomography of a genetically encoded near-infrared fluorescent probe. *Angew. Chem. Int. Ed. Engl.* 51, 1448–1451
58. Krumholz, A. *et al.* (2014) Multicontrast photoacoustic *in vivo* imaging using near-infrared fluorescent proteins. *Sci. Rep.* 4, 3939
59. Deliolanis, N.C. *et al.* (2014) Deep-tissue reporter-gene imaging with fluorescence and optoacoustic tomography: a performance overview. *Mol. Imaging Biol.* 16, 652–660
60. Yao, J. *et al.* (2016) Multiscale photoacoustic tomography using reversibly switchable bacterial phytochrome as a near-infrared photochromic probe. *Nat. Methods* 13, 67–73
61. Shcherbakova, D.M. *et al.* (2015) Molecular basis of spectral diversity in near-infrared phytochrome-based fluorescent proteins. *Chem. Biol.* 22, 1540–1551
62. Baloban, M. *et al.* (2017) Designing brighter near-infrared fluorescent proteins: insights from structural and biochemical studies. *Chem. Sci.* 8, 4546–4557
63. Goedhart, J. *et al.* (2010) Bright cyan fluorescent protein variants identified by fluorescence lifetime screening. *Nat. Methods* 7, 137–139
64. Repina, N.A. *et al.* (2017) At light speed: advances in optogenetic systems for regulating cell signaling and behavior. *Annu. Rev. Chem. Biomol. Eng.* 8, 13–39
65. Rost, B.R. *et al.* (2017) Optogenetic tools for subcellular applications in neuroscience. *Neuron* 96, 572–603
66. Hochbaum, D.R. *et al.* (2014) All-optical electrophysiology in mammalian neurons using engineered microbial rhodopsins. *Nat. Methods* 11, 825–833
67. Emiliani, V. *et al.* (2015) All-optical interrogation of neural circuits. *J. Neurosci.* 35, 13917–13926

68. Entcheva, E. and Bub, G. (2016) All-optical control of cardiac excitation: combined high-resolution optogenetic actuation and optical mapping. *J. Physiol.* 594, 2503–2510

69. Barykina, N.V. *et al.* (2016) A new design for a green calcium indicator with a smaller size and a reduced number of calcium-binding sites. *Sci. Rep.* 6, 34447

70. Hock, A.K. *et al.* (2017) Development of an inducible mouse model of iRFP713 to track recombinase activity and tumour development *in vivo*. *Sci. Rep.* 7, 1837

71. Tran, M.T. *et al.* (2014) *In vivo* image analysis using iRFP transgenic mice. *Exp. Anim.* 63, 311–319

72. Lin, M.Z. *et al.* (2009) Autofluorescent proteins with excitation in the optical window for intravital imaging in mammals. *Chem. Biol.* 16, 1169–1179

73. Wannier, T.M. *et al.* (2017) Monomerization of far-red fluorescent proteins. *bioRxiv* Published online July 20, 2017. http://dx.doi.org/10.1101/162842

74. Cranfill, P.J. *et al.* (2016) Quantitative assessment of fluorescent proteins. *Nat. Methods* 13, 557–562

75. Rumyantsev, K.A. *et al.* (2016) Near-infrared bioluminescent proteins for two-color multimodal imaging. *Sci. Rep.* 6, 36588

76. Rice, W.L. *et al.* (2015) *In vivo* tomographic imaging of deep-seated cancer using fluorescence lifetime contrast. *Cancer Res.* 75, 1236–1243

77. Tzoumas, S. *et al.* (2015) Effects of multispectral excitation on the sensitivity of molecular optoacoustic imaging. *J. Biophotonics* 8, 629–637

78. Li, L. *et al.* (2018) Small near-infrared photochromic protein for photoacoustic multi-contrast imaging and detection of protein interactions *in vivo*. *Nat. Commun.* 9, 2734

79. Telford, W.G. *et al.* (2015) Multiparametric flow cytometry using near-infrared fluorescent proteins engineered from bacterial phytochromes. *PLoS One* 10, e0122342